Stormier mid-Holocene southwest Indian Ocean due to poleward trending tropical cyclones

Green, A.N.[1,2], Cooper, J.A.G. [2,1], Dixon, S.[1], Loureiro, C.[3,1], Hahn, A.[4], Zabel, M.[4]

[1]Geological Sciences, School of Agricultural, Earth and Environmental Sciences, University of KwaZulu-Natal, Westville Campus, Private Bag X54001, South Africa

[2]School of Environmental Sciences, Centre for Coastal and Marine Research, Ulster University, Cromore Road, Coleraine BT52 1SA, UK

[3]Biological and Environmental Sciences, Faculty of Natural Sciences, University of Stirling, Stirling FK8 1XG, UK

[4]MARUM Center for Marine Environmental Sciences, University of Bremen, Bremen, Germany

Abstract

Geological evidence of past storminess is fundamental in contextualising long-term climate variability and investigating future climate. Unlike the Atlantic and Pacific basins, robust storminess reconstructions do not exist for most of the Indian Ocean, despite the hazard tropical cyclones pose to the SE African margin. Here we combine seismic stratigraphy with analysis of marine sediment cores to look for regionally representative storm-related sediment deposits –or tempestites- intercalated in shoreface sediments from the SW Indian Ocean off South Africa. Tempestites, represented by hummocky seismic units, whose sediments have clear marine geochemical signatures, are found to have been deposited between 6.5 and 4.6 cal kyr BP, when sea level was

between 0 and + 3 m above present. Deposition and preservation of the tempestites reflect unprecedented tropical cyclone impacts, associated with periods of strongly positive Indian Ocean Dipole (IOD) anomalies and linked to warmer sea surface temperatures. Future climate projections suggest stronger positive IOD anomalies and further intensification and poleward migration of tropical cyclones, like their mid-Holocene predecessors. Given the rarity of tropical cyclone landfalls in South Africa, this urges revaluation of hazards in areas along the southeast African coast likely to become more vulnerable to landfalling tropical cyclones in future.

Palaeoclimatic reconstructions are vital in understanding past and future climate trends. Because of the high impact of storms in coastal areas, climate projections often include simulations of future storminess. Whereas many lines of evidence provide records of past temperatures, pre-instrumental evidence of storminess is less abundant[1]. Several high-magnitude tropical storms (Hurricane Katrina, Cyclone Nargis, Hurricane Sandy, Typhon Haiyan) in recent decades reveal the inadequacy of the instrumental record to characterise storm recurrence intervals for exceptionally high-impact events. Evidence of past storms and stormy periods is preserved in various marine geological proxies including: (i) the paralic zone (washover deposits in back-barrier marsh sediments[2] and erosional scarps in emergent barriers[3]), (ii) the shoreface and shelf (storm deposits or tempestites)[4,5] and (iii) deep ocean sediments (coarse-grained layers in pelagic sequences)[6]. These storminess proxies have the potential to extend the instrumental record if adequate chronological control can be established. To date, paralic and deep ocean sediments have received most attention in this regard whereas shelf and shoreface tempestites have long been recognised, but little used in palaeo-tempestology. Storm deposits preserved in the shoreface or inner-shelf stratigraphy are effective tools to assess the largest magnitude storms, however, their preservation potential is low as they can potentially be reworked by subsequent storm events. When preserved, tempestites provide a standing record of the largest storms, particularly intense tropical cyclones[7], and set a benchmark against which contemporary and future storminess can be assessed.

While the links between climate variability and tropical cyclone frequency, intensity and track are nowadays better constrained[8], uncertainties remain due to the limited availability and quality of historical records and variations between modelling studies[9]. Considering the sea surface temperature (SST) threshold (26.5°C) required for tropical storms to develop[10], ocean warming under a changing climate will lead to an expansion of areas of tropical cyclone formation, consistent with the poleward displacement of intensity maxima of tropical cyclones over the past decades[11]. However, there is low confidence in projected changes for tropical cyclone genesis, track and duration, despite the likely decrease in frequency and increase in intensity[9], and there is particularly low confidence in basin-specific projections of storminess and associated storm surges[12].

Part of the reason for this uncertainty is the lack of palaeo-tempest records against which to compare climate model outputs, which need to be extended both in time and space[8]. Various records of palaeo-tempests from the Pacific and Atlantic Oceans[7,13] have been linked to modes of climate variability such as the NAO, ENSO or the PDO[14]. No such records of palaeo-tempests have been reported from the coasts of the SW Indian Ocean despite the known impacts of regular tropical cyclones[15,16,17,18]. Here we present evidence from tempestites preserved on the lower shoreface off Durban, South Africa (29.9° S, 31.0° E) (Fig. 1), which record a period of enhanced storminess during the mid-Holocene. We assesses the timing, genesis and preservation of the tempestites and their association with tropical cyclones and climate variability for the SE African coast, providing a benchmark for future assessment and modelling of tropical cyclone-climate links[19] in the Indian Ocean.

Shoreface tempestites in the SW Indian Ocean

Along the microtidal, wave-dominated east coast of southern Africa, which is exposed to a range of tropical and extratropical cyclones driving extreme storm waves, sea level has risen episodically over the last 18 kyrs[20,21]. It reached the present level ~ 6 kyrs BP, after which two minor highstands (+3.5 and +1.5 m) occurred at 4.5 and 1.6 kyrs BP (Fig. 1b). Offshore Durban (South Africa), the lower shoreface (between fair- and storm-weather wave base[22]), is characterised by Holocene unconsolidated transgressive sediments that mantle and abut occasional aeolianite pinnacles[23]. Here, we present the seismic stratigraphy and age-controlled sedimentary and geochemical analysis of two cores (see Methods) collected during RV METEOR Cruise M102[24].

The sedimentary succession intersected by cores GeoB18304-1 and GeoB18303-2 (Fig.1) comprises three units (1-3) that overlie and postdate the Holocene wave ravinement[23] (Fig. 2). The succession imaged occupies the mid-shelf where the sediment cover is thin and patchy, each unit separated in space but necessarily in time. The contemporary depth of storm wave sediment reworking is estimated at ~ 40 m[25], just below which these three units occur. The sandy nature and position of the units identify them as part of the contemporary lower shoreface[23].

The lower shoreface comprises a seaward Unit 1 that consists of irregular, wavy to chaotic high-amplitude reflectors (e.g. Fig. 2a, Extended Data Fig. 1a). Unit 2 comprises two facies: a proximal set of flat-lying reflectors that become progradational with depth (2A) (Extended data Fig. 1a), onlapped by hummocky, wavy to irregular and chaotic reflectors (2B, Fig. 2b), all of which are truncated by Surface ii (Extended data Fig. 1b, Fig. 2). This surface is irregular and is overlain by Unit 3, which comprises another series of irregular, wavy to chaotic high-amplitude reflectors and forms the shallowest accumulation of the lower shoreface (Fig. 2b). Units 1 and 2 are separated by zones of non-deposition, marked by exposed erosional surfaces and aeolianite pinnacles at -55 to -60 m (Extended data Fig. 1).

The seaward core (GeoB18303-2) in 60 m water depth contains a uniform succession of shelly, medium to coarse sands (Fig. 3a). Seismic unit 1 is intersected by the upper 3.5 m of the core. This unit is characterised by the presence of several mudballs between 1.8 and 3 m depth. These date from 12 052 cal yr BP in the lower sections followed by a significant hiatus between 11 224 cal yr and 4177 cal yr BP when the most recent deposition of mudballs occurred (Fig. 3a).

The landward core (GeoB18304-1) in 35 m water depth shows a general fining-upward succession from a series of pebbly coarse sands to medium sand that correlates to Unit 2B (Fig. 3b). The lower portion of the core comprises a series of coarse grained, sharp-topped and sharp-based event beds. No datable material was found at their upper boundary, but ages below and above date from 6980 cal yr BP to a minimum of 2619 cal yr BP (Fig. 3b). The uppermost part of the core correlates with Unit 3 and comprises a coarsening upward succession of coarse to very coarse sands.

The most significant changes in grain size and element concentration in core GeoB18303-2 occur between 1.5 m and 2.25 m (Fig. 3c and d). Here significant decreases in the concentration of the marine fraction elements including Ca (103.76 g/kg) and Sr (174 mg/kg) are evident, with corresponding finer grain sizes (Fig 3c). Associated with these depths are increases in the terrigenous fraction elements including Si (204.91 g/kg), Al (41.57 g/kg), K (15.97 g/kg), Ti (319 mg/kg) and Rb (7 mg/kg), as well as an increase in Fe (20.15 g/kg). These coincide with the matrix that hosts the mudballs (Fig. 3d).

Grain size and elemental concentrations in core GeoB18304-1 vary little with depth until 3.15 m (Fig. 3e and f). From 3.15 m down to the basal layers, there is a significant scatter with multiple switching between high and low concentrations. There are multiple spikes in abundance of the marine elements towards the core base (Fig. 3f). The increases in marine elemental abundances are associated with the coarsest grain sizes that form the base of the small-scale, fining-upwards packages (Fig. 3b).

Potential mobilization of seafloor sediments based on modelled bed shear stress during extreme storm waves offshore Durban (see Methods) indicate that coarse sand, the most common material found in both cores, is mobilized over the entire domain (Extended Data Fig. 2a). The thresholds for mobilization of gravel-sized sediments (Extended Data Fig. 2b), the coarsest material found in the proximal cores, are similarly exceeded along the entire lower shoreface. For the 100 yr return-period storm, the entire shoreface and inner shelf would be subject to disturbance for both classes of coarse sediment (Extended Data Fig. 2c,d).

Storm deposits

The shoreface units (1-3) post-date the early Holocene wave ravinement surface identified by previous authors[23]. Unit 1 onlaps the various aeolianite/beachrock ridges as a series of seaward-thinning wedges of shelly sediment with notably irregular, wavy to chaotic high-amplitude reflectors. Distally, unit 1 comprises mudballs within a very coarse sand matrix. The terrestrial origin of the mudballs is indicated by high Ti abundance (Fig. 3d). They occur within a coarse-grained shell hash with high marine elemental signatures. Mudballs on the shelf are commonly found in storm-dominated settings where the coastline is undergoing transgressive erosion. They are derived through storm-driven erosion of muddy coastal/fluvial sediments and subsequent offshore transport in storm-return flows that extend below storm wave base[26,27]. The mud is likely derived from an outcropping or subcropping source on the adjacent foreshore. This occurs presently in the study area, when storm erosion exposes laterally continuous back-barrier mud layers along the shoreline[28]. Based on their terrestrial signatures and transgressively eroding setting, we consider the mudballs to represent similar storm-based erosion of terrestrial-sourced muds from the foreshore and subsequent deposition within the tempestite sequence in the lower shoreface, as a result of storm return flows. No further mudballs occurred in the upper stratigraphy of either of the cores. The dated outer layer of the mudball (4117 cal yr BP) reflects the maximum age of deposition of this material on the shelf.

Unit 2 is present at depths from 60 to 40 m (Extended Data Fig. 1), with isolated pockets of sub-Unit 2B occurring at the termini of the prograding sub-Unit 2A. The high abundance of marine fraction elements, separated by finer material with high terrigenous elemental abundance are indicative of periodic high-energy marine events[29,30]. The marine-dominated shell and pebble hash horizons are similar to deposits ("rippled scour depressions") associated with storm scour on the inner shelf[31,32,33]. The small-scale, sharp-based coarse packages that terminate with terrestrial element-rich sands are similar to the tempestites described by others[26]. Sub-Unit 2B is thus considered to comprise a series of storm-generated gravel/sand couplets.

Dates from the overlying Unit 3 constrain the deposition of the overlying shoreface sediments to 2619 cal yr BP and 1878 cal yr BP. Units 1 and 2B, and the storm intervals they record, span two distinct time periods. The distal storm deposits (mudballs in storm return flow deposits) date from 12 052 cal yr BP to 11 224 cal yr BP, followed by a hiatus, to 4 177 cal yrs BP. The more proximal storm deposits more closely match this younger date, and span the 6 980 cal yr BP to 4910 cal yr BP interval. In the context of palaeo-sea levels, the timing of deposition of the older tempestites is associated with a time when sea levels were ~ 30-45 m below mean sea level[21,34] (Fig. 1), whereas the proximal group occurred when sea level was between 0 and + 3 m[21] (Fig. 1). The older and distal storm deposits were initially associated with a lowered wave base (~ -45 to -60 m from 12 to 11 ka), at which time and based on their depths, they likely developed in upper shoreface-hosted rippled scour depressions. As sea level rose to the present, periodic storm deposition continued on the outer shoreface until 4 177 cal yr BP.

The proximal deposits relate entirely to deposition below storm wave base under contemporary sea level conditions[25]. Preservation potential of tempestites is low because subsequent storms rework older deposits[35], but intense tropical cyclones generate thick shoreface deposits that can survive physical and biological reworking[36].

While the largest of contemporary storms recorded in the coast of Durban appears capable of remobilising gravel-sized particles over the entire lower shoreface (Extended Data Fig. 2), the tempestite horizons are still preserved in the substrata. The storm deposits thus appear to record events of a magnitude that has not been exceeded since. We attribute this to intense tropical storms given the geographical position of Durban in relation to the Southern Indian Ocean tropical cyclone belt[37]. In the overlying succession of shoreface sediments, there are no further storm event horizons, suggesting no further impingement by intense storms capable of forming such pervasive tempestites on the seabed.

Similar sequences of tempestites have been associated with centennial to millennial periods of increased tropical cyclone activity in the Atlantic Ocean[7,38], produced by landfall of hurricanes of category 3 and higher. While tropical cyclones of such intensity have not made landfall along the eastern coast of South Africa in the past 5 decades[18,37,39], and less intense (category 1 and 2) tropical cyclones rarely make landfall along this coastline[40], the tempestites archived in the cores and seismic stratigraphy point to a prolonged mid-Holocene period of very intense tropical cyclone activity in southern Africa.

Paleo-climatic context

The mid-Holocene tempestite record of core GeoB18304-1 indicates that intense storm activity started at or before the oldest date the core (6980 cal yrs BP) and was ongoing at least until the youngest date (4816 cal yrs BP). Studies elsewhere suggest that intense storminess is likely to be associated with increased regional SST[41], which in the western

Indian Ocean is related to the IOD[42]. The IOD is considered a major climatic driver across the Indian Ocean region throughout the Holocene[43]. Positive IOD events are associated with greater-than-average SST in the western Indian Ocean and increased rainfall over East Africa[44]. Positive IOD anomalies occur when strong easterly winds and weakening of eastward oceanic currents along the equatorial Indian Ocean facilitate atmospheric and oceanic current reversals[45,46,47]. The majority of studies of atmospheric and oceanic circulation in the Indian Ocean link rapid SST warming in the west to strong easterly winds and weakening of eastward oceanic currents along the equatorial Indian Ocean. Enhanced convection over the Indian Ocean reflects a positive IOD anomaly[48]. Large changes in the monsoon rainfall in the eastern Indian Ocean have been attributed to the occurrence of strong positive IOD anomalies[49,50], during which SST is high and the likelihood of intense and more frequent tropical cyclones in the western Indian Ocean increases. Strong positive IOD induces extreme weather events in eastern Africa[51], and is associated with increased rainfall along the coasts of Mozambique and South Africa[52].

This period coincides with strong positive IOD events that caused aridity and SST cooling over the eastern Indian Ocean, while the western margin experienced increased precipitation and positive SST anomalies[53,54,55,56]. When compared to Mauritian climate records (Fig. 4b), the tempestite deposition matches an overall period of negative IOD state with strong positive anomalies[57]. This period is further correlated with records offshore Somalia[58] and Tanzania[43] which reveal warmer SST for the western Indian Ocean between 7.8 and 4.7 ka BP (Fig. 4c). Higher SST not only increases the likelihood of intense and more frequent tropical cyclones, but also contributes to a southward shift in the latitudinal position of the 26 ºC and 27 ºC isotherms, and potential changes in the location of tropical cyclone landfalls, tracking south of Madagascar and making landfall in higher latitude regions along the coasts of Mozambique and South Africa[16]. After 4.3 ka the lack of tempestites is also associated with a shift towards a stronger El Niño and a less prominent Eastern Indian Ocean monsoon since 3600 BP[54] (Fig. 4d).

Examinations regarding changes to tropical cyclone frequency and intensity over the southern Indian Ocean under a warming climate have been inconclusive and often contradictory[9,17,39,59,60]. However, an increasing trend in the intensity and duration of tropical cyclones associated with warming SST and upper ocean heat content in the southern Indian Ocean has been observed in the last two decades[18]. Under high greenhouse emission scenarios, multi-model climate projections robustly indicate more frequent[61] and more intense[51] strong positive IOD events, driven by increased SST variability in the western Indian Ocean. Therefore, global warming will likely lead to enhanced storminess in Southern Africa, linked to strong positive IOD events associated with more intense and southward tracking tropical cyclones, of which the mid-Holocene deposits on the Durban shelf provide a clear analogue.

These findings demonstrate the potential of shoreface deposits as a proxy for past storminess and intense tropical-cyclone landfall. Two phases of enhanced storminess are recorded. One is associated with an early Holocene sea-level of ca. -40 m and is preserved in a drowned shoreface. The second (6.9 to 4.8 ka) is associated with contemporary sea-levels and records a period of enhanced storminess that, alongside other proxies, evidences a clear association with strong positive IOD events. Higher

SST and strong positive IOD events due to global warming are likely to lead to more intense, frequent and southward tracking tropical cyclones, whose impacts will be significantly greater than those of the present and the historic past along the coast of southern Africa.

Author Contributions Statement

AG led the paper conceptualisation, data collection, analysis, figure drafting, and together with JAGC managed the paper writing and editorial review. SD performed the laboratory analyses and figure drafting. CL performed the modelling and assisted in data analysis, writing, figure drafting and editorial review. AH and MZ assisted with data collection, writing, editorial review, with MZ the principal funding recipient.

Competing Interests Statement

The authors declare no competing interests.

Data availability

Samples and data (inorganic data, radiocarbon analyses) are respectively archived at the GeoB Core Repository and Pangaea (www.pangaea.de) both located at MARUM, University of Bremen. Modelling results are available on request of the corresponding author.

Figure captions

Figure 1. Location of the Durban shelf and study site with multibeam bathymetry[20] (courtesy eThekweni Municipality), seismic coverage (grey lines) and core sites. Inset **b,** SE African sea level curve[21]. SA=South Africa, Moz = Mozambique, Tan =

Tanzania, Ken = Kenya, Som = Somalia, Sey = Seychelles, Maur = Mauritius. Map projection WGS84, UTM 36S

Figure 2. Zoomed in ultra-high-resolution seismic stratigraphy of the lower shoreface. **a)** core site GeoB18303-2. **b,** GeoB18304-1. Note the hummocky nature of unit 2B intersected by GeoB18304-1. Profile positions of a and b denoted in figure 1 and the full profiles are provided in Extended Data Fig. 1. WRS = wave ravinement surface

Figure 3. Downcore variations and chronology. **a,** GeoB1803-2. **b,** GeoB18304-1. Areas of interest are outlined by shaded grey boxes. WRS = Holocene wave ravinement surface. **c,** bulk sediment grain size variations GeoB1803-2. **d,** downcore elemental distributions GeoB1803-2. **e,** bulk sediment grain size variations GeoB1804-1. **f,** downcore elemental distributions GeoB1804-1. Grey lines link spikes in grain size with corresponding peaks and troughs in marine and terrestrial material. Cl = clay, Si = silt, VFS = very fine sand, FS = fine sand, MS = medium sand, CS = coarse sand, VCS = very coarse sand, P = pebbles, Gr = granules, Co = cobbles, B =boulders

Figure 4. Lithologic and geochemical variations compared to major climatic oscillations in the South West Indian Ocean (SWIO). **a,** downcore variations of grain size, Ca and Ti abundances and geochronology of GeoB18304-1, **b,** fluctuating Ca/Ti ratios in cores from Mauritius[57], **c,** SST anomalies (lines) from Tanzania[43] and reconstructed alkenone palaeothermometry SST data from Tanzania (circles)[58], **d,** El Niño events per 100 years[62]. Red circles are strong El Niño Indian Ocean Dipole (IOD) events, blue circles are strong monsoon IOD events, grey blocks denote period of interest. ENSO = El Niño-Southern Oscillation

References

1. Oliva, F., Viau, A. E., Peros, M. C., and Bouchard, M. 2018. Paleotempestology database for the western North Atlantic basin. The Holocene, 28(10), 1664–1671.
2. Donnelly, J.P. Roll, S. Wengren, M. Butler, J. Lederer, R. Webb T. 2001. Sedimentary evidence of intense hurricane strikes from New Jersey. Geology, 29, 615-618.
3. Buynevich, I.V., FitzGerald, D.M., van Heteren, S. 2004. Sedimentary records of intense storms in Holocene barrier sequences, Maine, USA Marine Geology 210, 135-148
4. Siringan, J.W., Anderson, J.B., 1994. Modern shoreface and inner-shelf storm deposits off the east Texas coast, Gulf of Mexico. Journal of Sedimentary Research B64, 99-110.
5. Tamura, T., Masuda, F., 2005. Bed thickness characteristics of inner□shelf storm deposits associated with a transgressive to regressive Holocene wave□dominated shelf, Sendai coastal plain, Japan. Sedimentology 52, 1375-1395.
6. Toomey, M. R., Curry, W. B. Donnelly, J. P. van Hengstum P. J. 2013. Reconstructing 7000 years of North Atlantic hurricane variability using deep-sea sediment cores from the western Great Bahama Bank, Paleoceanography 28, 31–41
7. Donnelly, J.P. and Woodruff, J.D., 2007. Intense hurricane activity over the past 5,000 years controlled by El Niño and the West African monsoon. Nature, 447(7143), 465-468.

8. Walsh, K.J.E., McBride, J.L., Klotzbach, P.J., Balachandran, S., Camargo, S.J., Holland, G., Knutson, T.R., Rossin, J.P., Lee, T., Sobel, A., Sugi, M., 2016. Tropical cyclones and climate change. WIRES Climate Change 7, 65-89. DOI: 10.1002/wcc.371
9. Knutson, T.R., McBride, J.L., Chan. J., Emanuel, K., Holland, G., Landsea, C., Held, I., Kossin, J.P., Srivastava, A.K., Sugi, M., 2010, Tropical cyclones and climate change. Nature Geoscience 3, 157-163.
10. Tory, K.J. and R.A. Dare, 2015. Sea Surface Temperature Thresholds for Tropical Cyclone Formation. J. Climate, 28, 8171–8183
11. Kossin, J.P., Emanuel, K.A., Vecchi., G.A., 2014. The poleward migration of the location of tropical cyclone maximum intensity. Nature 509, 349-352.
12. Kirtman, B., S.B. Power, J.A. Adedoyin, G.J. Boer, R. Bojariu, I. Camilloni, F.J. Doblas-Reyes, A.M. Fiore, M. Kimoto, G.A. Meehl, M. Prather, A. Sarr, C. Schär, R. Sutton, G.J. van Oldenborgh, G. Vecchi and H.J. Wang, 2013: Near-term Climate Change: Projections and Predictability. In: Climate Change 2013: The Physical Science Basis. Contribution of Working Group I to the Fifth Assessment Report of the Intergovernmental Panel on Climate Change [Stocker, T.F., D. Qin, G.-K. Plattner, M. Tignor, S.K. Allen, J. Boschung, A. Nauels, Y. Xia, V. Bex and P.M. Midgley (eds.)]. Cambridge University Press, Cambridge, United Kingdom and New York, NY, USA.
13. Nott, J., Hayne, M., 2001. High frequency of "super-cyclones" along the Great Barrier Reef over the past 5,000 years. Nature 413, 508-512.
14. Liu, K., 2013. Paleotempestology. In: Encyclopedia of Quaternary Science, 2nd Edition. Eds S.A. Elias, C.J. Mock. Elsevier, Amsterdam, 209–221.

15. Ash, K.D., Matyas, C.J., 2012. The influences of ENSO and the subtropical Indian Ocean Dipole on tropical cyclone trajectories in the southwestern Indian Ocean. International Journal of Climatology, 32(1), 41-56.

16. Fitchett, J.M. and Grab, S.W., 2014. A 66□year tropical cyclone record for south□east Africa: temporal trends in a global context. International Journal of Climatology, 34, 3604-3615.

17. Muthige, M.S., Malherbe, J., Engelbrecht, F.A., Grab, S., Beraki, A., Maisha, T.R., Van der Merwe, J., 2018. Projected changes in tropical cyclones over the South West Indian Ocean under different extents of global warming. Environmental Research Letters 13, 065019. DOI: 10.1088/1748-9326/aabc60

18. Vidya, P.J., Ravichandran, M., Murtugudde, R., Subeesh, M.P., Chartejee, S., Neetu, S., Nuncio, M., 2021. Increased cyclone destruction potential in the Southern Indian Ocean. Environmental Research Letters, 16 (1), 014027.

19. Frappier, A, Knutson, T, Liu, K-B, Emanuel, K., 2007 Perspective: coordinating paleoclimate research on tropical cyclones with hurricane-climate theory and modelling. Tellus A 59, 529–537.

20. Green, A.N., Cooper, J.A.G., Salzmann, L., 2014. Geomorphic and stratigraphic signals of postglacial meltwater pulses on continental shelves. Geology 42(2), 151-154.

21. Cooper, J.A.G., Green, A.N. and Compton, J. 2018. Sea-level change in southern Africa since the last glacial maximum. Quaternary Science Reviews, 201, 303-318.

22. Hamon-Kerivel, K., Cooper, J.A.G, Jackson, D.W.T., Sedrati, M., Pintado, E.G., 2020. Shoreface mesoscale morphodynamics: A review. Earth-Science Reviews, 209, p.103330

23. Pretorius, L., Green, A.N., Cooper, J.A.G. (2016). Submerged shoreline preservation and ravinement during rapid post glacial sea-level rise and subsequent slowstand. Bulletin of the Geological Society of America 128, 1059-1069.

24. Eckau, W. (2014). Short cruise report RV Meteor—M102. Retrieved from https://www.ldf.uni□hamburg.de/meteor/wochenberichte/wochenberichte□meteor/m101□m103/m102□scr.pdf

25. Smith, A.M., Mather, A.A,, Bundy, S.C., Cooper, J.A.G., Guastella, L.A., Ramsay, P.J., Theron, A., 2010. Contrasting styles of swell-driven coastal erosion: examples from KwaZulu-Natal, South Africa. Geological Magazine, 147(6), 940-953.

26. Walker, R.G., Plint, A.G., 1992. Wave- and storm-dominated shallow marine systems. In Walker, R.G., and James, N.P., (eds). Facies models: response to sea-level changes. St. John's, Newfoundland, Canada, Geological Association of Canada, 219-238.

27. Hampson, G. J., Storms, J. E. A., 2003. Geomorphological and sequence stratigraphic variability in wave-dominated, shoreface-shelf parasequences. Sedimentology 50(4), 667-701.

28. Cooper, J.A.G., Mason, T., 1986. Barrier Washover Fans in the Beachwood Mangrove Area, Durban, South Africa: cause, morphology and environmental effect. Journal of Shoreline Management 2, 285-303.

29. Morton, R.A., Gelfenbaum, G., Jaffe, B.E., 2007. Physical criteria for distinguishing sandy tsunami and storm deposits using modern examples. Sedimentary Geology 200(3), 184-207.
30. Goff, J., Chagué-Goff, C., Nichol, S., Jaffe, B., Dominey-Howes, D., 2012. Progress in palaeotsunami research. Sedimentary Geology, 243–244: 70–88. DOI:10.1016/j.sedgeo.2011.11.002.
31. Murray, A.B., Thieler, E.R., 2004. A new hypothesis and exploratory model for the formation of large-scale inner-shelf sediment sorting and "rippled scour depressions". Continental Shelf Research 24(3), 295-315.
32. Goff, J.A., Mayer, L.A., Traykovski, P., Buynevich, I., Wilkens, R., Raymond, R., Glang, G., Evans, R.L., Olson, H., Jenkins, C., 2005. Detailed investigation of sorted bedforms, or "rippled scour depressions," within the Martha's Vineyard Coastal Observatory, Massachusetts. Continental Shelf Research, 25(4), 461-484.
33. Trembanis, A. C., T. M. Hume., 2011. Sorted bedforms on the inner shelf off northeastern New Zealand: Spatiotemporal relationships and potential paleo-environmental implications, Geo Marine Letters 31(3), 203-214. DOI: 10.1007/s00367-010-0225-8.
34. Peltier, W.R., Fairbanks, R.G., 2006. Global glacial ice volume and Last Glacial Maximum duration from an extended Barbados sea level record. Quaternary Science Reviews 25(23-24), 3322–3337
35. Keen, T.R., Bentley, S.J., Vaughan, W.C., Blain, C.A., 2004. The generation and preservation of multiple hurricane beds in the northern Gulf of Mexico. Marine Geology 210 (1-4), 79-105. DOI: 10.1016/j.margeo.2004.05.022

36. Bentley, S.J., Keen, T.R., Blain, C.A. and Vaughan, W.C., 2002. The origin and preservation of a major hurricane event bed in the northern Gulf of Mexico: Hurricane Camille, 1969. Marine Geology, 186(3-4), pp.423-446.

37. Ramsay, A.H., Camargo, S.J., Kim, D., 2012. Cluster analysis of tropical cyclone tracks in the Southern Hemisphere. Climate Dynamics 39, 897-917.

38. van Hengstum, P.J., Donnelly, J.P., Toomey, M.R., Albury, N.A., Lane, P., Kakuk, B., 2014. Heightened hurricane activity on the Little Bahama Bank from 1350 to 1650 AD. Continental Shelf Research 86, 103-115.

39. Fitchett, J.M., 2018. Recent emergence of CAT5 tropical cyclones in the South Indian Ocean. South African Journal of Science 114 (11/12), 4426, 6 p.

40. Reason, C., Keibel, A., 2004. Tropical cyclone Eline and its unusual penetration and impacts over the Southern African mainland. Weather and Forecasting 19, 789-805.

41. Webster, P.J., Holland, G.J., Curry, J.A., Chang, H.R., 2005. Changes in Tropical Cyclone Number, Duration, and Intensity in a Warming Environment. Science 309(5742), 1844-1846. DOI: 10.1126/ science.1116448.

42. Saji, N.H., Goswami, B.N., Vinayachandran, P.N., Yamagata, T., 1999. A dipole mode in the tropical Indian Ocean. Nature 401, 360-363.

43. Kuhnert, H., Kuhlmann, H., Mohtadi, M., Meggers, H., Baumann, K.-H., P€atzold, J., 2014. Holocene tropical western Indian Ocean sea surface temperatures in covariation with climatic changes in the Indonesian region. Paleoceanography 29, 423-437. DOI: 10.1002/2013PA002555.

44. Webster, P.J., Moore, A.M., Loschnigg, J.P., Leben, R.R., 1999. Coupled ocean-atmosphere dynamics in the Indian Ocean during 1997-98. Nature 401, 356-360. DOI: 10.1038/43848.
45. Vecchi, G. A., Soden, B. J., 2007. Global warming and the weakening of the tropical circulation. Journal of Climatology 20(17), 4316-4340.
46. Cai, W., Zheng, X.T., Weller, E., Collins, M., Cowan, T., Lengaigne, M., Yu, W., Yamagata, T., 2013. Projected response of the Indian Ocean Dipole to greenhouse warming. Nature Geoscience 6, 999-1007.
47. Zheng, X.T., Xie, S.P., Du, Y., Liu, L., Huang, G., Liu, Q., 2013. Indian Ocean dipole response to global warming in the CMIP5 multimodel ensemble. Journal of Climate, 26(16), 6067-6080.
48. Ding, R., Li, J., 2012. Influences of ENSO teleconnection on the persistence of sea surface temperature in the tropical Indian Ocean. Journal of Climate, 25(23), 8177-8195.
49. Gadgil, S., Vinayachandran, P.N., Francis, P.A., Gadgil, S., 2004. Extremes of the Indian summer monsoon rainfall, ENSO and equatorial Indian Ocean oscillation. Geophysical Research Letters 31(12), L12213. DOI: 10.1029/2004GL019733.
50. Deshpande, A., Chowdary, J.S., Gnanaseelan, C., 2014. Role of thermocline SST coupling in the evolution of IOD events and their regional impacts. Climate Dynamics 43(1), 163-174.
51. Cai, W., Yang, K., Wu, L., Huang, G., Santoso, A., Ng, B., Wang, G., Yamagata, T., 2021. Opposite reponse of strong and moderate positive Indian Ocean Dipole to global warming. Nature Climate Change, 11, 27-32.

52. Reason, C.J.C. , 2001. Subtropical Indian Ocean SST dipole events and southern African rainfall. Geophysical Research Letters, 28(11), 2225-2227.

53. Wang, Y., Cheng, H., Edwards, R.L., He, Y., Kong, X., An, Z., Wu, J., Kelly, M.J., Dykoski, C.A., Li, X., 2005. The Holocene Asian Monsoon: links to solar changes and North Atlantic climate. Science 308(5723), 854-857. DOI: 10.1126/science.1106296.

54. Abram, N.J., Gagan, M.K., Liu, Z., Hantoro, W.S., McCulloch, M.T., Suwargadi, B.W., 2007. Seasonal characteristics of the Indian Ocean Dipole during the Holocene epoch. Nature 445(7125), 299-302.

55. Fleitmann, D., Burns, S.J., Mangini, A., Mudelsee, M., Kramers, J., Villa, I., Neff, U., Al Subbary, A.A., Buettner, A., Hippler, D., Matter, A., 2007. Holocene ITCZ and Indian monsoon dynamics recorded in stalagmites from Oman and Yemen (Socotra). Quaternary Science Reviews 26(1-2), 170-188.

56. Mohtadi, M., Oppo, D.W., Steinke, S., Stuut, J.B.W., De Pol Holz, R., Hebbeln, D., Luckge, A., 2011. Glacial to Holocene swings of the Australian-Indonesian monsoon. Nature Geoscience 4, 540-544.

57. De Boer, E.J., Tjallingii, R., Vélez, M.I., Rijsdijk, K.F., Vlug, A., Reichart, G.J., Prendergast, A.L., de Louw, P.G., Florens, F.V., Baider, C. and Hooghiemstra, H., 2014. Climate variability in the SW Indian Ocean from an 8000-yr long multi-proxy record in the Mauritian lowlands shows a middle to late Holocene shift from negative IOD-state to ENSO-state. Quaternary Science Reviews, 86, pp.175-189.

58. Bard, E., Rostek, F., Sonzogni, C., 1997. Interhemispheric synchrony of the last deglaciation inferred from alkenone palaeothermometry. Nature, 385(6618), 707-710.

59. Malherbe, J., Engelbrecht, F.A., Landman, W.A., 2013. Projected changes in tropical cyclone climatology and landfall in the Southwest Indian Ocean region under enhanced anthropogenic forcing. Climate Dynamics 40, 2867-2886.

60. Holland, G., Bruyere, C.L., 2014. Recent intense hurricane response to global climate change. Climate Dynamics 42, 617-627.

61. Cai, W., Santoso, A., Wang, G., Weller, E., Wu, L., Ashok, K., Masumoto, Y., Yamagata, T., 2014. Increased frequency of extreme Indian Ocean Dipole events due to greenhouse warming. Nature 510, 254-258.

62. Moy, C.M., Seltzer, G.O., Rodbell, D.T., Anderson, D.M., 2002. Variability of El Niño/Southern Oscillation activity at millennial timescales during the Holocene epoch. Nature, 420(6912), 162-165.

Acknowledgements

This work was financially supported by the Bundesministerium für Bildung und Forschung (BMBF, Germany) within the project “Regional Archives for Integrated Investigations (RAiN, 03G0840A)” (MZ). We thank the captain, crew and scientists of the METEOR M102 cruise for facilitating the recovery of the studied material, and eThekwini Municipality for access to multibeam bathymetry.

Corresponding author: Andrew Green greena1@ukzn.ac.za

Extended Data Fig. 1. Seismic reflection profiles and interpretations of the seismic stratigraphy of the Durban shelf. **a,** full record including figure 2a. **b,** full record including figure 2b.

Extended Data Fig. 2. Bed shear stress represented according to the thresholds for sediment mobility. Model results for the largest recorded storm offshore Durban for: **a**, coarse sand, **b**, fine gravel, and the 100 yr return-period storm for **c**, coarse sand, **d**, fine gravel. Areas below threshold are blanked. Note that at the GeoB18304-1 site, granule-size sediment would be mobilised, but not at the GeoB18303-2 site.

Methods

Regional setting: The eastern coast of South Africa is characterised by mean annual significant wave height of 1.65 m[63], and spring and neap tidal ranges are between ~ 1.8 m and ~0.5 m, respectively[64]. Extreme waves in this coastal area are driven by tropical cyclones, mid-latitude (extratropical) cyclones and cut-off lows[63,65]. If tropical cyclones become stationary south east of Madagascar they can drive large wave events along the east coast of South Africa[63,65], while cut-off low systems may also drive large waves storm waves and surges. No tropical cyclones made landfall in the coast of South Africa since wave records began in the early 1980’s, but an intense cut-off low system occurred in March 2007. The storm generated the largest waves recorded, with peak significant wave height of 8.5 m, corresponding to a return-period of 32 to 61 years[66]. This event caused widespread coastal erosion and infrastructural damage[25].

Geophysical surveying and coring: The shallow sub-surface geology was examined using ultra-high-resolution 0.5kHz PARASOUND collected during RV METEOR Cruise M102 in December 2013[24]. All data were processed by high and low band pass filtering and gain application and exported as SEGY data for visualisation in the Kingdom Suite software package. The processed PARASOUND data resolve to ~ 10 cm in the vertical domain with a maximum penetration of ~ 20 m in localised areas. In all lines, the upper 5 m of the seafloor sediment package were resolved with a high level of detail. Key targets were identified from the ultra-high-resolution seismic packages for coring. Three vibrocores were collected during the same cruise[24], two of which (GeoB18303-2 and GeoB18304-1) are described in this study (Fig. 1). Previous descriptions of the seismic stratigraphy are included together with those of this study in Supplementary Table 1. Multibeam bathymetry[67] collected by the eThekweni Municipality were integrated with the ultra-high resolution seismic and core data in order to assess the spatial distribution of tempestite signatures on the lower Durban shoreface.

Laboratory analysis: Cores were split onboard and logged according to standard sedimentological procedures. Sub-sampling at 5cm intervals for grain size and geochemical analyses was undertaken, together with sampling for material suitable for Accelerator Mass Spectrometry (AMS) 14C dating. A total of 13 samples were collected from cores GeoB18303-2 and GeoB18304-1 for dating purposes. The material used for AMS 14C dating is listed in Extended Data Fig. 3. All shell material was selected from in-situ life position, especially in the case of bivalves that were still articulated. Wherever possible, the most intact shells were chosen with the least amount of bleaching of the shell exterior. All dates are corrected for reservoir effect with a ΔR of 121 ± 16 14C yr[68]. The dates discussed in this manuscript are median values; the two sigma ranges are indicated in Supplementary Table 2.

Particle size analysis was undertaken for both the bulk and terrigenous sediment fractions. The samples were sieved to obtain the bulk grain size distribution with the result of the analysis presented as phi values where the mean, median, sorting and skewness were calculated using the Folk and Ward equations. For the terrigenous grain fractions, the sediment samples were treated with 10% HCl, H_2O_2 and NaOH to remove calcium carbonate, organic matter, and biogenic opal, respectively. The samples were then suspended in demineralised water with the addition of $Na_4P_2O_7$ to prevent the formation of aggregates. The particle size distribution was measured with a Coulter laser particle sizer LS 13 320 (MARUM, University of Bremen, Germany) generating 92 size classes from 0.4 to 2000 µm. For this study the mean grain-size data are displayed as phi.

Additional samples were collected at selected locations corresponding to significant results obtained from the grain size analyses. Sample pre-treatment consisted of drying and grinding for 120 seconds in a silicon nitride vessel to prevent contamination (Planetary Micro Mill PULVERISETTE 7 premium line, MARUM, University of Bremen, Germany), to assure that all particles were smaller than 63 µm.

Elemental compositions were measured on 205 sediment samples where 4 grams of each sample compressed at 25 kPa, were used to analyse for major, minor and trace element composition by X-Ray Fluorescence spectrometry (Panalytical epsilon 3 XL, Bremen University, Germany). USGS and Chinese rock and sediment standard reference material GBW 07316 was measured simultaneously and gave results within +- 3-5% of certified values.

Wave modelling and sediment mobility analysis: Shoreface sediment mobility in response to storm wave forcing was analysed using the nearshore wave propagation model SWAN version 41.20AB[69.70]. Simulations of the wave field were performed for the maximum wave conditions during the largest storm recorded offshore Durban[63] (March 2007; significant wave heigh of 8.5 m and peak wave period of 16.6 s) and for the 100-year return period storm[66] (significant wave height of 10.3 m and peak period of 17.4 s). SWAN is a depth and phase-averaged, third-generation wave model that simulates de refractive propagation and evolution of the wave spectrum. The model was run in stationary mode, i.e. time is removed from the computations and waves are assumed to propagate instantaneously across the modelling domain, using default parameters in order to account for bottom friction dissipation, non-linear wave interaction, diffraction and white-capping dissipation[71]. A regular structured grid with 5 meters resolution was used for representing the computational domain, matching the bathymetric grid used to represent the bottom conditions (Fig. 1).

Considering the dependency of near-bed sediment movement on the bottom orbital velocity amplitude[72], outputs from SWAN included the root-mean-square of the orbital motion near the bottom (U_{rms}) for the entire modelling domain, computed considering a JONSWAP spectral shape and empirical bottom friction model and linear wave theory[73]. To evaluate the potential for wave-induced coarse sediment entrainment and transport during modelled storm conditions, the threshold bed shear stress for initiation of sediment transport (T_{cr}) based on the modified Shields parameter was computed[72] for coarse sand (d_{50}= 0.5 to 2mm) and fine gravel (d_{50}=2 to 8 mm)[74]. T_{cr} values of 0.63 N/m^2 and 4.00 N/m^2 were obtained for the mean class values of coarse sand (d_{50} = 1.25 mm) and fine gravel (d_{50} = 5 mm), respectively.

These values were then compared to the spatially variable bed shear stress under waves (T_{ws}), considering that on a flat, non-rippled bed typical of coarse sediments, the bed shear stress can be simplified and only the wave-skin friction component (T_{ws}) is required to determine the hydrodynamic forcing acting on the bed and driving sediment entrainment and transport[72]. T_{ws} was computed using modelled bottom orbital velocity ($U_w = U_{rms}$) and the wave friction factor (f_w) according to:

$$T_{ws} = \tfrac{1}{2} p f_w U_w^2$$

where p is seawater density (1027 kg/m^3), U_w corresponds to U_{rms} modelled with SWAN and f_w computed using the formulation[72]:

$$f_w = 1.39(A/z_0)^{-0.52}$$

where A is the semi-orbital excursion ($U_w T/2\pi$), and z_0 the bed roughness length ($d_{50}/12$).

Data availability

Seismic and core data (geochemical, grain size and chronology) are available at Pangaea (www.pangaea.de). Modelling data are available on request from AG or CL.

Methods references:

63. Corbella, S., Stretch D., 2012a. The wave climate on the KwaZulu-Natal coast of South Africa. Journal of the South African Institution of Civil Engineering 54(2), 45-54.

64. Moes, H., Rossouw, M., 2008. Considerations for the utilization of wave power around South Africa. Workshop on Ocean Energy, Centre for Renewable and Sustainable Energy Studies, Stellenbosch, 21, February 2008, Abstracts.

65. Mather, A.A., Stretch, D.D., 2012. A perspective on sea level rise and coastal storm surge from Southern and Eastern Africa: a case study near Durban, South Africa. Water, 4(1), 237-259

66. Corbella S., Stretch D., 2012b. Multivariate return periods of sea storms for coastal erosion risk assessment. Natural Hazards and Earth System Sciences, 12, 2699-2708.

67. Green, A.N., Dladla, N. and Garlick, G.L., 2013. Spatial and temporal variations in incised valley systems from the Durban continental shelf, KwaZulu-Natal, South Africa. Marine Geology, 335, pp.148-161.

68. Maboya, M., Meadows, M., Reimer, P., Backeberg, B., & Haberzettl, T. (2018). Late Holocene Marine Radiocarbon Reservoir Correction for the Southern and Eastern Coasts of South Africa. Radiocarbon, 60(2), 571-582. doi:10.1017/RDC.2017.139

69. Booij N., Ris R.C., Holthuijsen L.H., 1999. A third-generation wave model for coastal regions - 1. Model description and validation. Journal of Geophysical Research, 104, 7649–7666.

70. Ris RC, Holthuijsen LH, Booij N. 1999. A third-generation wave model for coastal regions - 2. Verification. Journal of Geophysical Research, 104, 7667–7681.

71. Loureiro C., Ferreira Ó., Cooper J.A.G., 2012. Extreme erosion on high-energy embayed beaches: influence of megarips and storm grouping. Geomorphology, 139–140, 155–171.

72. Soulsby R. 1997. Dynamics of Marine Sands: a manual for practical applications. Thomas Telford, London, 280p.

73. Holthuijsen L.H., 2007. Waves in Oceanic and Coastal Waters. Cambridge University Press: Cambridge.

74. Blott S., Pye K., 2012. Particle size scales and classification of sediment types based on particle size distributions: review and recommended procedures. Sedimentology, 59, 2071-2096.

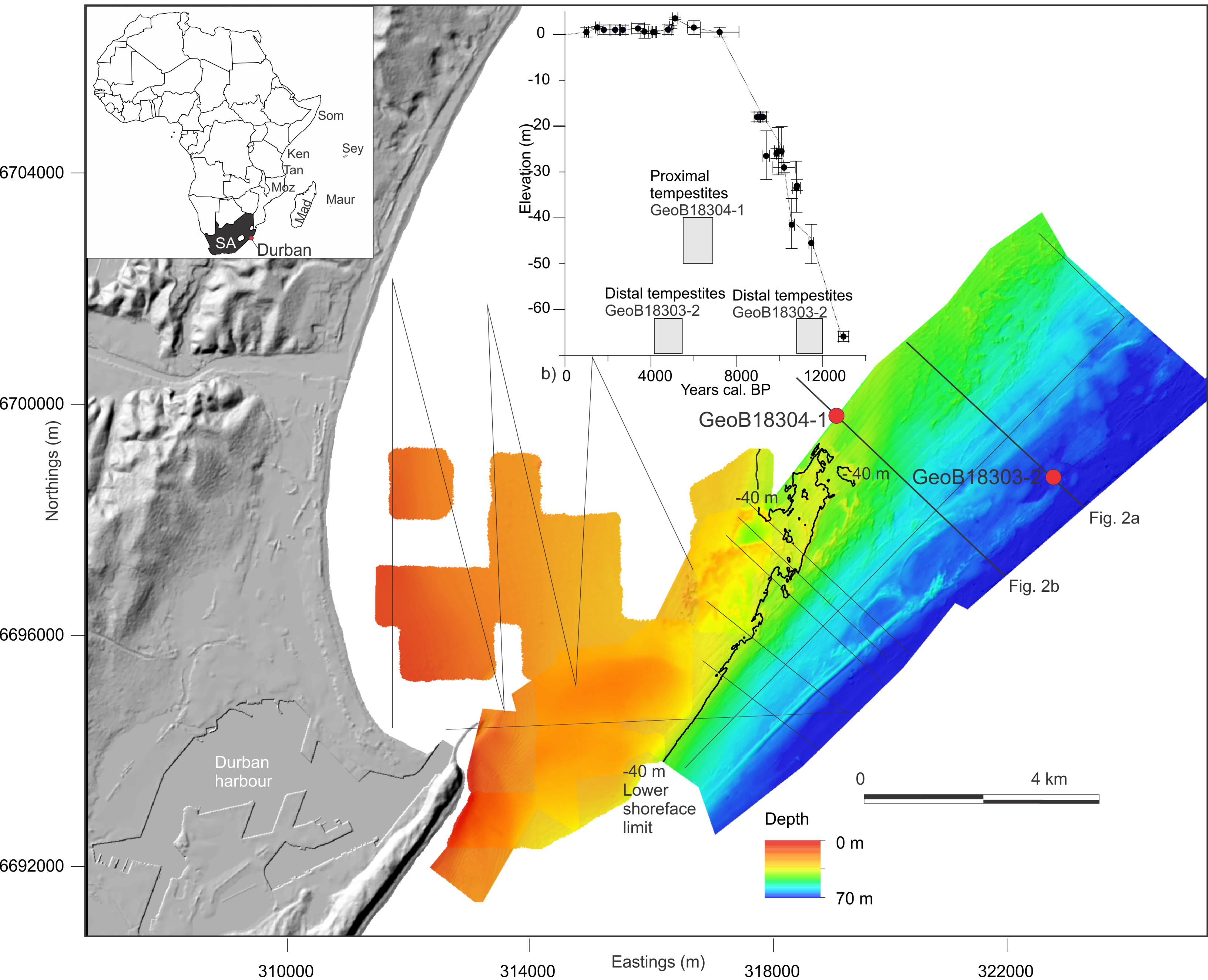

Som
Sey
Ken
Tan
Moz
Maur
Mad
SA
Durban
0
-10
-20
-30
-40
-50
-60
Elevation (m)
Proximal tempestites
GeoB18304-1
Distal tempestites
GeoB18303-2
Distal tempestites
GeoB18303-2
b)
0
4000
8000
12000
Years cal. BP
GeoB18304-1
-40 m
-40 m
GeoB18303-2
Fig. 2a
Fig. 2b
Durban harbour
-40 m
Lower shoreface limit
0
4 km
Depth
0 m
70 m
6704000
6700000
6696000
6692000
Northings (m)
310000
314000
318000
322000
Eastings (m)

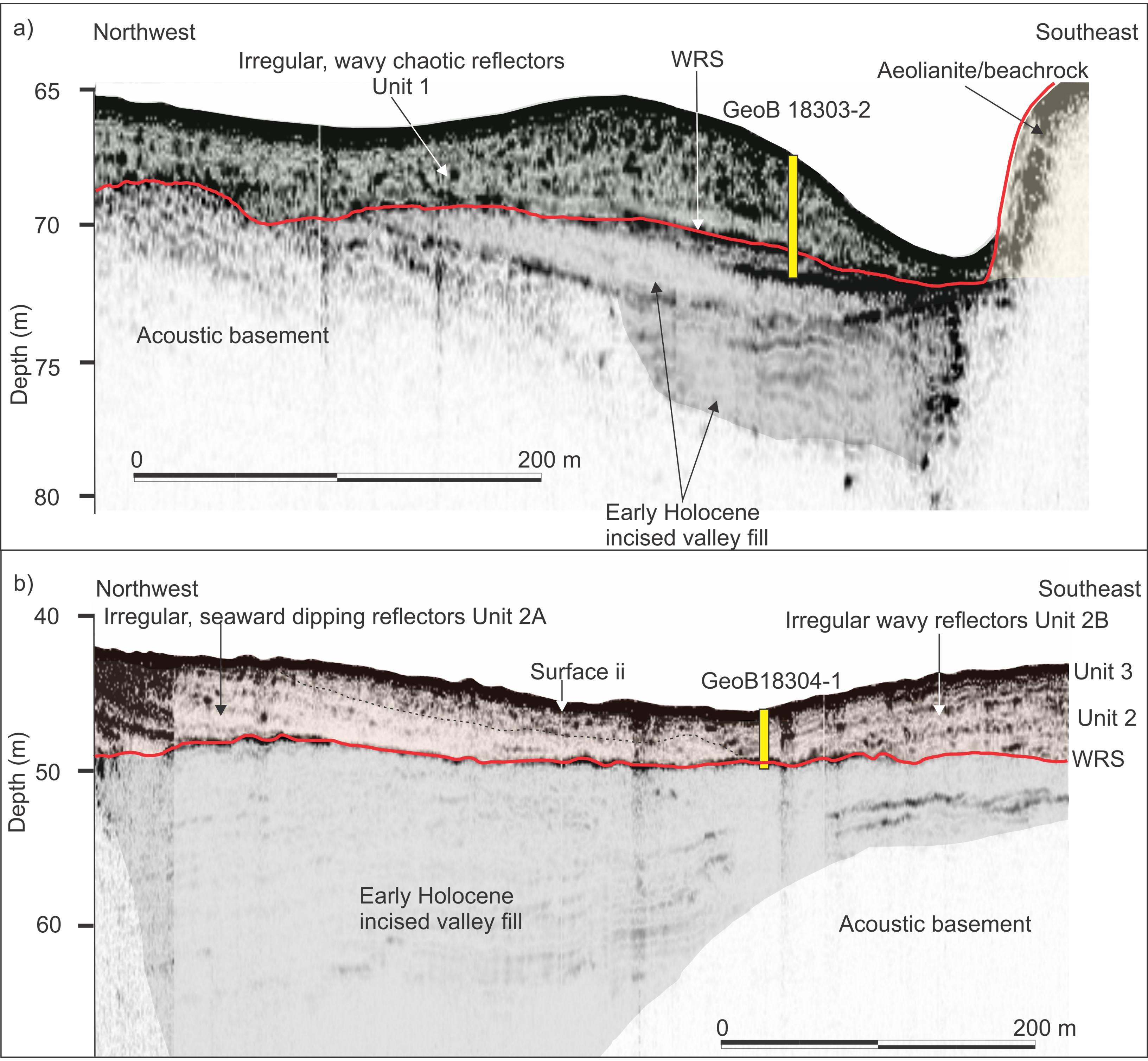
a)
Northwest
Southeast
Irregular, wavy chaotic reflectors
Unit 1
WRS
Aeolianite/beachrock
GeoB 18303-2
65
70
75
80
Depth (m)
Acoustic basement
0
200 m
Early Holocene
incised valley fill
b)
Northwest
Southeast
40
Irregular, seaward dipping reflectors Unit 2A
Irregular wavy reflectors Unit 2B
Surface ii
GeoB18304-1
Unit 3
Unit 2
WRS
50
60
Depth (m)
Early Holocene
incised valley fill
Acoustic basement
0
200 m

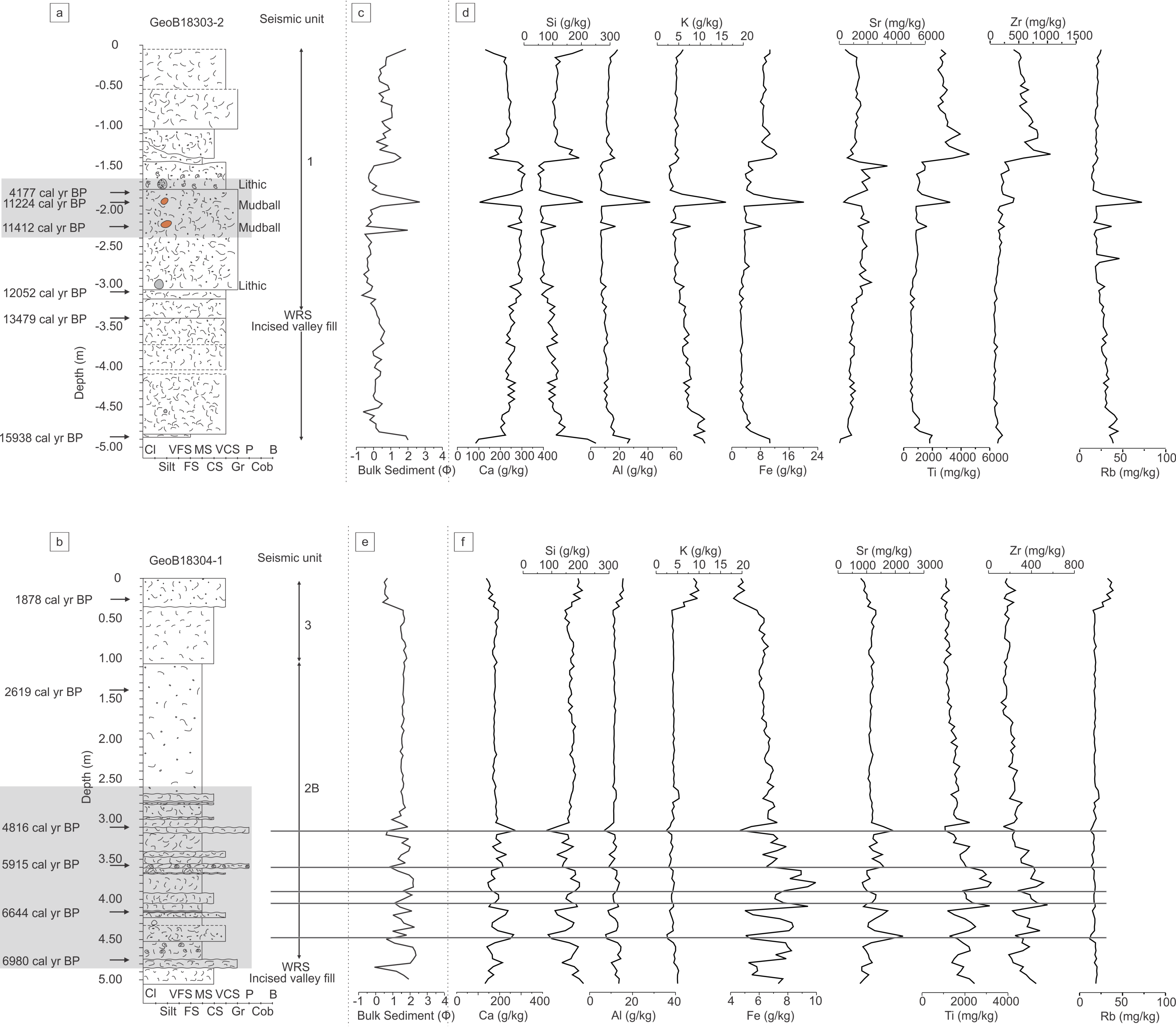

a
GeoB18303-2
Seismic unit
4177 cal yr BP
11224 cal yr BP
11412 cal yr BP
12052 cal yr BP
13479 cal yr BP
15938 cal yr BP
Lithic
Mudball
Mudball
Lithic
1
WRS
Incised valley fill
Depth (m)
Cl VFS MS VCS P B
Silt FS CS Gr Cob
c
Bulk Sediment (Φ)
d
Si (g/kg)
K (g/kg)
Sr (mg/kg)
Zr (mg/kg)
Ca (g/kg)
Al (g/kg)
Fe (g/kg)
Ti (mg/kg)
Rb (mg/kg)
b
GeoB18304-1
Seismic unit
1878 cal yr BP
2619 cal yr BP
4816 cal yr BP
5915 cal yr BP
6644 cal yr BP
6980 cal yr BP
3
2B
WRS
Incised valley fill
e
f

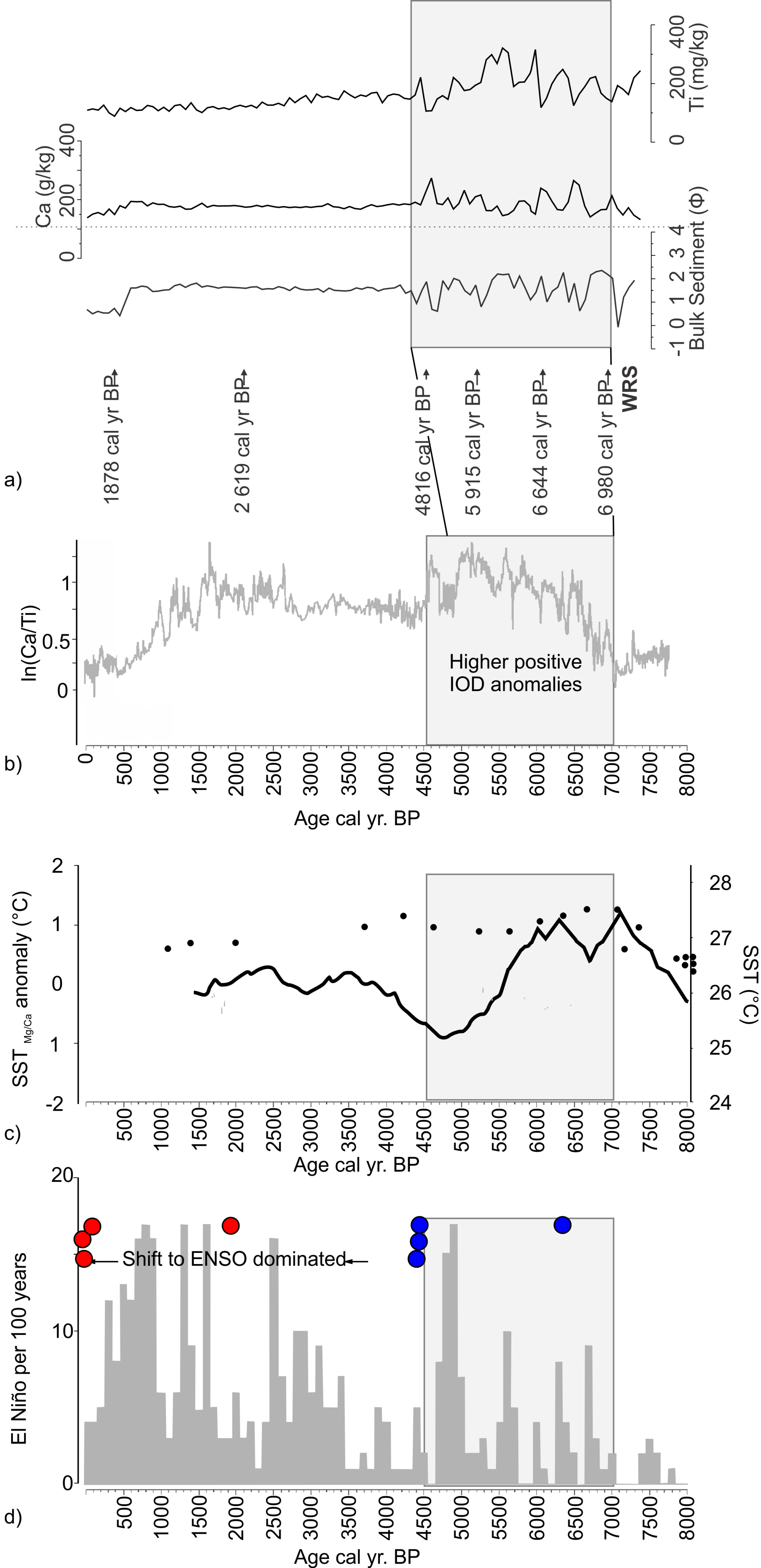

Ti (mg/kg)
0
200
400
Ca (g/kg)
0
200
400
Bulk Sediment (Φ)
-1 0 1 2 3 4
1878 cal yr BP
2 619 cal yr BP
4816 cal yr BP
5 915 cal yr BP
6 644 cal yr BP
6 980 cal yr BP
WRS
a)
ln(Ca/Ti)
0
0.5
1
Higher positive
IOD anomalies
b)
0 500 1000 1500 2000 2500 3000 3500 4000 4500 5000 5500 6000 6500 7000 7500 8000
Age cal yr. BP
SST Mg/Ca anomaly (°C)
2
1
0
1
-2
SST (°C)
24 25 26 27 28
c)
500 1000 1500 2000 2500 3000 3500 4000 4500 5000 5500 6000 6500 7000 7500 8000
Age cal yr. BP
El Niño per 100 years
0
10
20
Shift to ENSO dominated
d)
500 1000 1500 2000 2500 3000 3500 4000 4500 5000 5500 6000 6500 7000 7500 8000
Age cal yr. BP

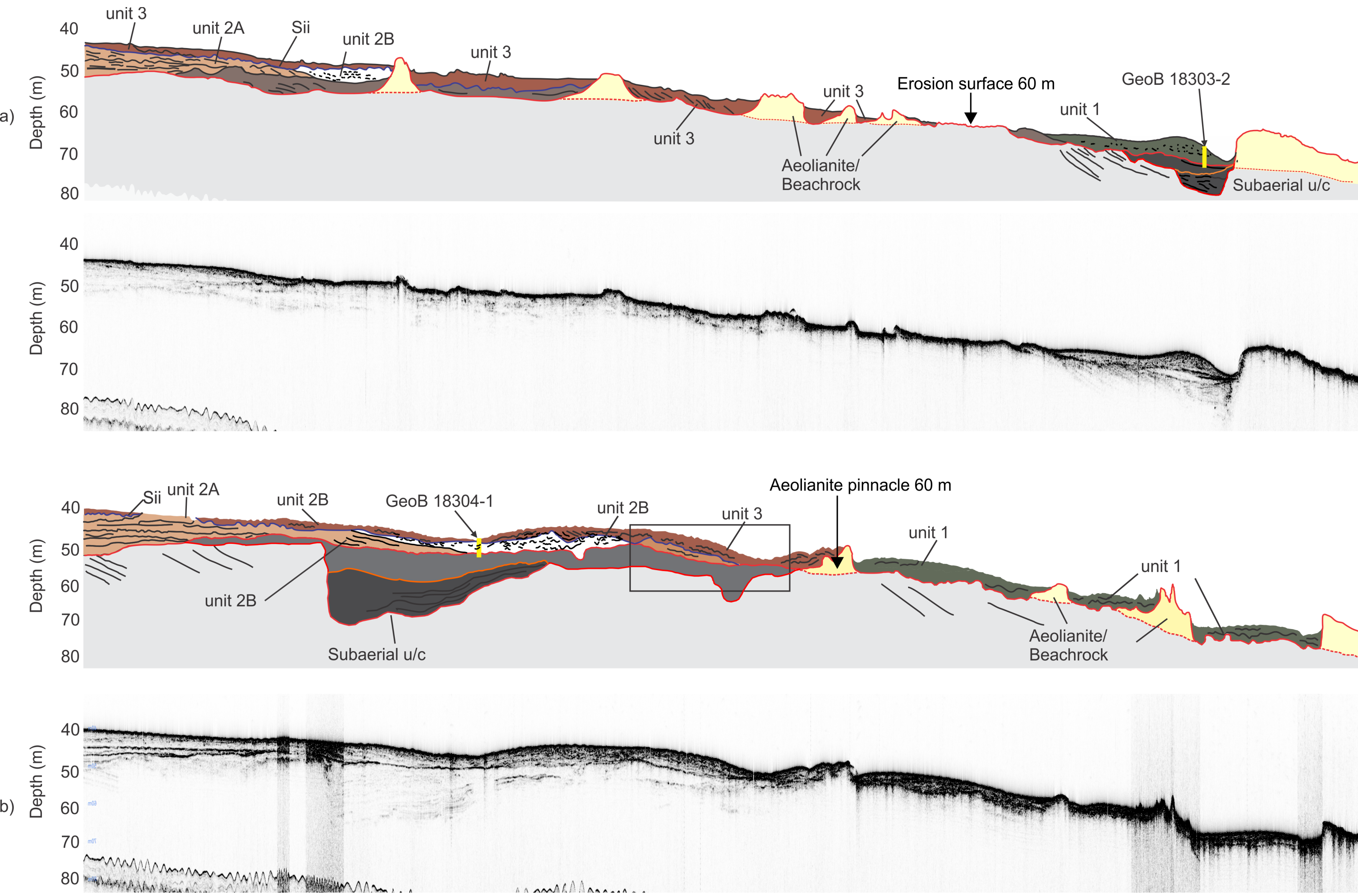

a)
b)
Depth (m)
40
50
60
70
80
unit 3
unit 2A
Sii
unit 2B
Erosion surface 60 m
GeoB 18303-2
unit 1
Aeolianite/
Beachrock
Subaerial u/c
GeoB 18304-1
Aeolianite pinnacle 60 m

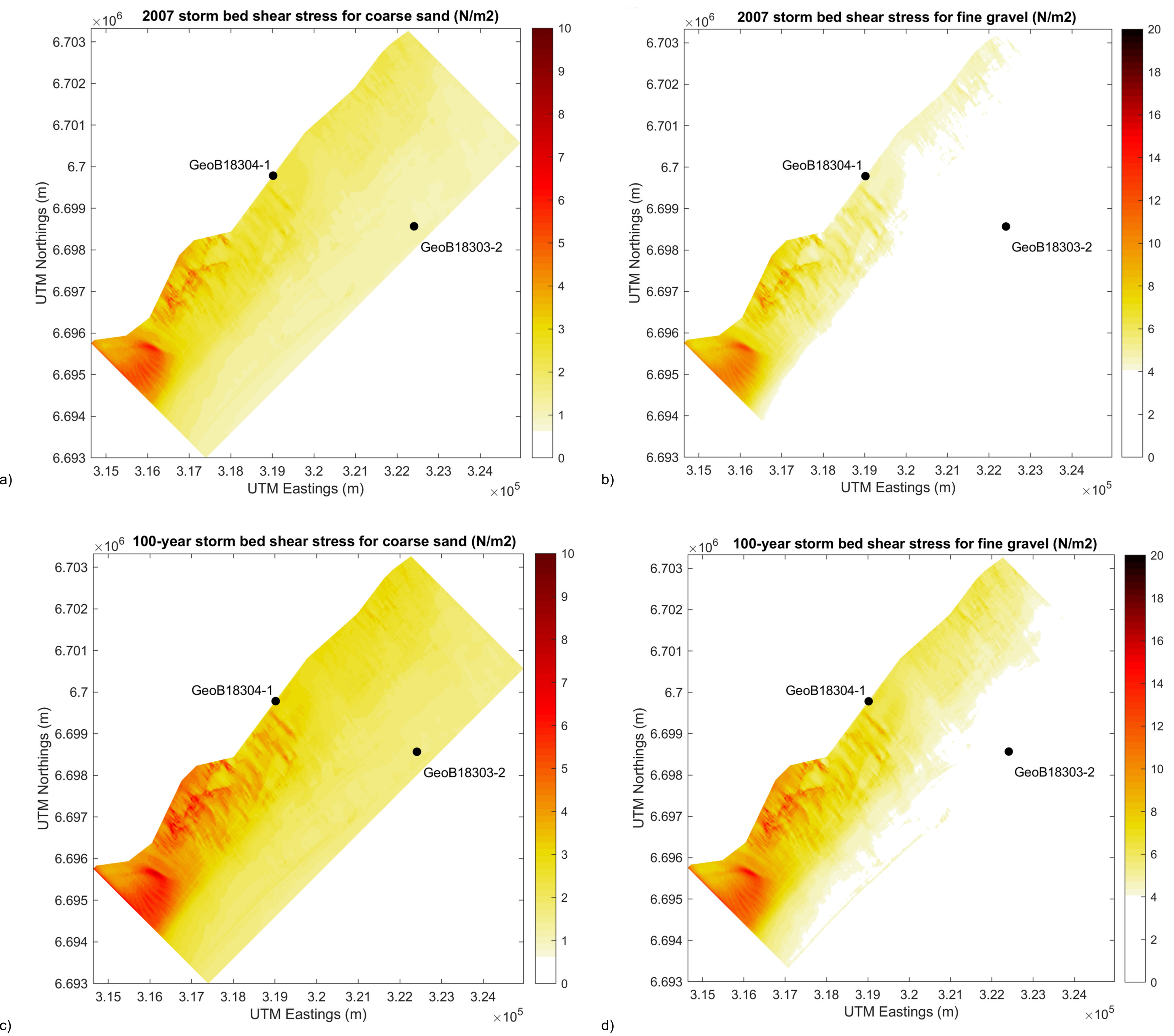

2007 storm bed shear stress for coarse sand (N/m2)
2007 storm bed shear stress for fine gravel (N/m2)
100-year storm bed shear stress for coarse sand (N/m2)
100-year storm bed shear stress for fine gravel (N/m2)
GeoB18304-1
GeoB18303-2
UTM Northings (m)
UTM Eastings (m)
×10^6
×10^5
a)
b)
c)
d)

Supplementary Table 2. Chronostratigraphy of GeoB18304-1 and GeoB18303-2. AMS radiocarbon dates are

Depth (cm)	**14C age yr BP**	**error ±**	**Material**
Core GeoB18304-1			
25	2 270	30	Bivalve
145	2 845	30	Single gastropod, Nassarius sp
310	4 595	35	Whole shell
359	5 530	40	Articulated bivalve, life position, Eumarcia paupercula
418	6 200	35	Articulated bivalve, life position, Eumarcia paupercula
476	6 480	40	Articulated bivalve, life position, Eumarcia paupercula
Core GeoB18303-2			
190	3 835	35	Bulk organic carbon (outer rim)
190	9 850	50	Bulk organic carbon (centre)
225	10 010	50	Bulk organic carbon
303	10 680	50	CaCO3
340	11 690	90	Bulk organic carbon
489	13 300	70	Bulk organic carbon

indicated, together with the composition of material dated and interpretation of the intersected unit/bracketing surfa

Interpretation (Unit/Surface)	Cal age yr BP	
	median	**+2σ**
Contemporary shoreface, unit 3	1878	1973
Storm-generated gravel/sand couplets, lower shoreface , unit 2	2619	2710
Storm-influenced sand lower shoreface, unit 2B	4816	4910
Storm-generated gravel/sand couplets, lower shoreface, unit 2B	5915	6017
Storm-generated gravel/sand couplets, lower shoreface, unit 2B	6644	6741
Storm-generated gravel/sand couplets, lower shoreface, unit 2B	6980	7127
Exterior of mudball, lower shoreface deposit, unit 1	4177	4383
Interior of mudball, lower shoreface deposit, unit 1	11224	1326
Mudball, lower shoreface deposit, unit 1	11412	11699
Reworked lower shoreface material, overlying wave ravinement surface, unit 1	12052	12346
Incised valley fill, flood tide deltaic package, underlying wave ravinement surface	13479	13583
Incised valley fill, flood tide deltaic package	15938	16180

ıce

-2σ	Calibration curve
1796	marine 13 (Reimer et al 2013)
2488	marine 13 (Reimer et al 2013)
4695	marine 13 (Reimer et al 2013)
5826	marine 13 (Reimer et al 2013)
6535	marine 13 (Reimer et al 2013)
6870	marine 13 (Reimer et al 2013)
3994	SHcal13 atmospheric curve (Hogg et al. 2013)
11138	SHcal13 atmospheric curve (Hogg et al. 2013)
11244	SHcal13 atmospheric curve (Hogg et al. 2013)
11827	SHcal13 atmospheric curve (Hogg et al. 2013)
13357	SHcal13 atmospheric curve (Hogg et al. 2013)
15707	SHcal13 atmospheric curve (Hogg et al. 2013)